

Deep Learning Superpixel Semantic Segmentation with Transparent Initialization and Sparse Encoder

Zhiwei Xu,^{1,2} Thalaiyasingam Ajanthan,¹ Richard Hartley¹

¹ Australian National University and Australian Centre for Robotic Vision, ² Data61, CSIRO
{firstname.lastname@anu.edu.au}

Abstract

Even though deep learning greatly improves the performance of semantic segmentation, its success mainly lies on object central areas but without accurate edges. As superpixel is a popular and effective auxiliary to preserve object edges, in this paper, we jointly learn semantic segmentation with trainable superpixels. We achieve it by adding fully-connected layers with transparent initialization and an efficient logit uniformization with a sparse encoder. Specifically, the proposed transparent initialization reserves the effects of learned parameters from pretrained networks, one for semantic segmentation and the other for superpixel, by a linear data recovery. This avoids a significant loss increase by using the pretrained networks, which otherwise can be caused by an inappropriate parameter initialization on the added layers. Meanwhile, consistent assignments to all pixels in each superpixel can be guaranteed by the logit uniformization with a sparse encoder. This sparse encoder with sparse matrix operations substantially improves the training efficiency by reducing the large computational complexity arising from indexing pixels by superpixels. We demonstrate the effectiveness of our proposal by transparent initialization and sparse encoder on semantic segmentation on PASCAL VOC 2012 dataset with enhanced labeling on the object edges. Moreover, the proposed transparent initialization can also be used to jointly finetune multiple or a deeper pretrained network on other tasks.

1 Introduction

Semantic segmentation is an essential and challenging task in computer vision of a pixel-level mapping between predefined semantics and image pixels of interesting objects. It has various applications in the real world, such as autonomous vehicles (Feng et al. 2020), object identification (Mottaghi et al. 2014; Salscheider 2019), image editing (Hong et al. 2018), scene analysis (Hofmarcher et al. 2019), and so on. Recent developments of semantic segmentation are greatly promoted by deep learning on several large-scale datasets, such as Berkeley segmentation benchmark (Martin et al. 2001) and the large-scale Microsoft Common Objects in Context 2017 (MS-COCO) (Lin et al. 2014), resulting in effective networks including FCN (Long, Shelhamer, and Darrell 2015), PSP (Zhao et al. 2017), CRFasRNN (Zheng et al. 2015), DeepLab serial (Chen et al. 2017, 2016, 2018a), etc. Although they are successful, the semantic labels are not substantially aligned with object edges (Long, Shelhamer,

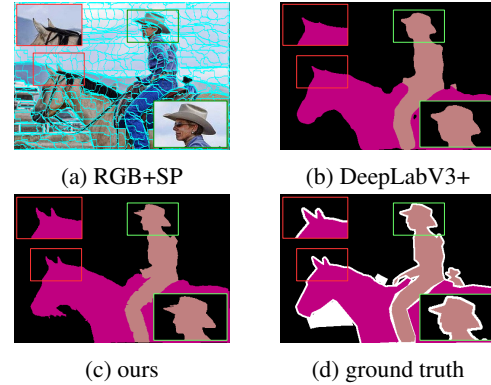


Figure 1: Example of enhanced semantic segmentation with sharp contours aligned with the superpixel (SP) map marked blue in (a). More results are in the experimental section.

and Darrell 2015; Zhao et al. 2017; Chen et al. 2018a).

This problem can be alleviated by works with qualified edge-aware preserving methods (Krahenbuhl and Koltun 2011; Zheng et al. 2015; Chen et al. 2017) or independently learning edges for semantic segmentation (Jampani et al. 2018; Gadde et al. 2016; Chen et al. 2016). Nevertheless, those edges are not always complete and usually over-segmented by learning with the artifact edge ground truth. Among these, denseCRF (Krahenbuhl and Koltun 2011) based methods are impressive in connecting object semantics over a large and dense range by bilateral filters via high-dimensional lattice computations. It could be more efficient and desirable to learn on locally oversegmented areas, such as superpixel that has been studied for years with a strong capability of aggregating similar contents into a higher-order clique (Achanta et al. 2012; Li and Chen 2015).

Existing superpixel segmentation approaches are mainly categorized into traditional methods, such as SLIC (Achanta et al. 2012), LSC (Li and Chen 2015), Crisp (Isola et al. 2014), BASS (Uziel, Ronen, and Freifeld 2019), and those in conjunction with modern neural networks, such as SSN (Jampani et al. 2018), affinity loss (Tu et al. 2018), superpixel by FCN (Yang et al. 2020). Although those traditional methods have qualified performance on superpixel segmentation, they cannot be easily embedded into neural networks for end-to-end learning due to the nondifferentiability or the

large computational complexity. In contrast, (Jampani et al. 2018) provides an end-to-end learning scheme for superpixel semantic segmentation, but the labeling assignments to pixels within the same superpixel differ from each other. This largely alleviates the value of superpixels for gathering pixels having similar properties of, for instance, intensities or features from CNN. Similarly, (Yang et al. 2020) adopts a simple fully convolutional network to learn superpixel segmentation for stereo matching, but the above problem will also occur when applied to semantic segmentation.

Hence, to deal with the problems of edge loss in semantic segmentation and inconsistent superpixel labeling, we cast the conjunction of these two networks with fully-connected layers with transparent initialization and logit uniformization. In more details, this transparent initialization maintains the effects of learned parameters of the pretrained networks by recovering the network output from its input at the early training stage, followed by a gradual divergence by learning from the auxiliary superpixels. Simultaneously, logit uniformization with sparse encoder enables a feasible and efficient logit averaging on pixels for each superpixel, which guarantees pixel semantics in each superpixel are consistent.

The main contributions of this work are:

- We jointly learn semantic segmentation and superpixel networks to enhance the labeling performance with sharp object edges. The enhancement is vivid with evaluations on the popular PASCAL VOC 2012 dataset.
- Transparent initialization is proposed for learning fused features by additional fully-connected layers on pretrained networks. This helps to joint and finetune networks without interrupting the effect of learned parameters of pretrained networks. Also, the transparent initialization is adoptable to finetune multiple or a deeper pretrained network for other tasks.
- Logit uniformization by a sparse encoder with sparse matrix operations ensures that the same semantic labeling is assigned to all pixels in each superpixel. The sparse matrix operations make it feasible for indexing pixels by superpixel to largely reduce the complexity. Otherwise, it is infeasible to execute the logit uniformization due to limited GPU memory in our experiments.

2 Related Work

Semantic segmentation. Semantic segmentation can be dated back to early techniques (Thoma 2016) based on classifiers, such as random decision forest (Schroff, Criminisi, and Zisserman 2008), SVM (Wang, Wang, and Bu 2011), and graphic models by MRF and CRF (Jordan 1998; Krahenbuhl and Koltun 2011). Such methods usually gather pixel sets with similar pixel colors, histogram of oriented gradients, textons, etc (Thoma 2016). In contrast, modern state-of-the-art methods rely on advanced exploitation on deep CNN classifier, such as ResNet (He et al. 2016), DenseNet (Huang et al. 2017), and VGG16 (Simonyan and Zisserman 2015). Fully Convolutional Network (FCN) (Long, Shelhamer, and Darrell 2015) related methods are typical architectures that leverage rich image features from

classifiers that are usually pretrained on ImageNet (Deng et al. 2009). SegNet (Badrinarayanan, Kendall, and Cipolla 2017) uses a U-Net structure for an encoder-decoder module to compensate for the low resolution by multiple upsampled feature maps. Then, several multi-scale contextual fusion methods (Chen et al. 2016; Lin et al. 2017; Chen et al. 2018a) are proposed to aggregate pyramid feature maps for fine-grained segmentation. Typically, DeepLabV3+ (Chen et al. 2018a) combines spatial pyramid pooling and encoder-decoder modules to refine the segmentation along with the object boundaries. Recently, some attention-based networks (Li et al. 2019; Zhao et al. 2018; Chen et al. 2018b; Fu et al. 2019) improve object labeling confidence by aggregating features of a single pixel from other positions.

Superpixel segmentation. Superpixel segmentation has been well studied for years with a comprehensive survey in (Stutz, Hermans, and Leibe 2018). Despite classical methods that initialize superpixel regions with seeds and clustering pixel sets by distance measurement (Wang et al. 2013), boundary pixel exchange (Bergh et al. 2015), etc., the widely-used SLIC based methods (Achanta et al. 2012; Liu et al. 2015; Li and Chen 2015; Achanta and Susstrunk 2017) employ (weighted) K-means clustering by pixel feature vectors to group neighbouring pixels. By deep learning, SSN (Jampani et al. 2018) first proposes an end-to-end learning framework for superpixel with differentiable SLIC for semantic segmentation and optical flow. Comparatively, (Yang et al. 2020) replaces the soft K-means manner in SSN by a simple fully convolutional network and applies it to stereo matching with downsampled and upsampled modules. While SSN results in superpixel-level semantic segmentation, the pixel labeling is not aligned with the superpixels. For instance, inconsistent labels exist in the same superpixel, which reduces the effects of superpixel on semantic assignments. This problem will also occur if (Yang et al. 2020) is directly applied to semantic segmentation.

Superpixel semantic segmentation. Some works adopt superpixels to optimize graph relations (Gould et al. 2014; Xing et al. 2016) or downsample images as a pooling alternative to max or average pooling (Gadde et al. 2016; Park et al. 2017; Schuurmans, Berman, and Blaschko 2018). These methods usually use fixed superpixels obtained by traditional methods mentioned in “superpixel segmentation” and lose the complete alignment of segmentation edges with the superpixel contours after upsampling. This, however, can be easily achieved by our logit uniformization module. Moreover, fixed superpixels are not suitable for end-to-end learning since traditional methods, such as SLIC (Achanta et al. 2012), are computationally expensive due to CPU execution and inflexible to fine-tune superpixels around the object edges, especially for small objects. Instead, learnable superpixels by CNN can alleviate this problem.

In sum, our proposal jointly learns superpixel semantic segmentation by fully exploiting the effect of superpixel on pixel-level labeling. Specifically, all pixels in the same superpixel share the same semantic label by the logit uniformization. Meanwhile, fully-connected layers with transparent initialization are used to fuse features from the pretrained networks, which will not interrupt the effect of the

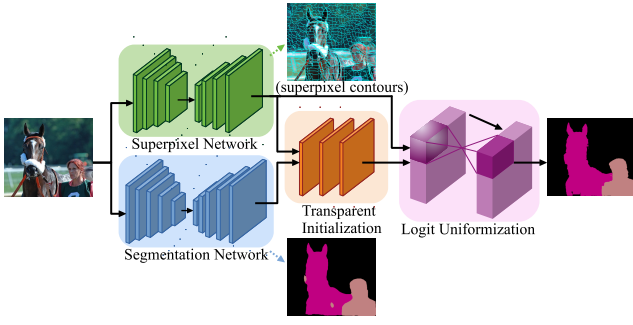


Figure 2: Flowchart of our proposal. “Transparent Initialization” consists of 3 fully-connected layers with an identity mapping, “logit uniformization” ensures pixel semantics are consistent within the superpixels. Best view in color.

learned parameters.

3 Methodology

3.1 Network Backbones

We adopt DeepLabV3+ (Chen et al. 2018a) with ResNet101/152 for semantic segmentation and superpixel with FCN (Yang et al. 2020) for superpixel segmentation.

DeepLabV3+ achieves high and robust performance with Atrous Spatial Pyramid Pooling (ASPP) for multi-scale feature maps and encoder-decoder modules for deep features by different output strides, followed by concatenations of upsampled low-level features to increase the image spatial resolution. It is widely used for semantic segmentation due to these modules that were evaluated by empirical studies. Readers can refer (Chen et al. 2018a) for more details.

Superpixel with FCN is used as our superpixel network. The core idea is to construct a distance-based loss function with mutual aggregations of neighbouring pixel and superpixel properties and location. This is similar to SLIC method (Achanta et al. 2012), where the property vectors can be CIELAB colors or one-hot encoding of semantic labels.

Given an image with N_p pixels and N_s superpixels, we denote the subsets of pixels as $\mathcal{P} = \{\mathcal{P}_0, \dots, \mathcal{P}_{N_s-1}\}$, where \mathcal{P}_i is a subset of pixels belonging to superpixel i . With pixel property $\mathbf{f} \in \mathbb{R}^{N_p \times K}$ (K features for each pixel) and probability map $\mathbf{q} \in \mathbb{R}^{N_s \times N_p}$ associated with surrounding superpixels, the loss function is

$$\mathcal{L}(\mathbf{f}, \mathbf{q}) = \sum_{p \in \mathcal{P}} E(\mathbf{f}(p), \mathbf{f}'(p)) + \frac{m}{D} \|\mathbf{c}(p) - \mathbf{c}'(p)\|_2 \quad (1)$$

with

$$\mathbf{u}_s = \frac{\sum_{p \in \mathcal{P}_s} \mathbf{f}(p) q_s(p)}{\sum_{p \in \mathcal{P}_s} q_s(p)}, \quad \mathbf{l}_s = \frac{\sum_{p \in \mathcal{P}_s} \mathbf{c}(p) q_s(p)}{\sum_{p \in \mathcal{P}_s} q_s(p)}, \quad (2a)$$

$$\mathbf{f}'(p) = \sum_{s \in \mathcal{N}_p} \mathbf{u}_s q_s(p), \quad \mathbf{c}'(p) = \sum_{s \in \mathcal{N}_p} \mathbf{l}_s q_s(p), \quad (2b)$$

where m is a weight balancing the effects of property and coordinates on loss, D is a superpixel sampling interval in proportion to superpixel size, $\mathbf{c}(i) = [x_i, y_i]^T$, $\forall i \in \{1, \dots, N_p\}$ are an image pixel coordinates, and $E(*)$ is a distance measure function by l_2 norm or cross-entropy function.

Here, \mathbf{u}_s and \mathbf{l}_s are superpixel-level property vector and central coordinates aggregated from involved pixels, respectively, and \mathbf{f}' and \mathbf{c}' are pixel-level property and coordinates aggregated from surrounding superpixels. This strategy updates between pixels and superpixels till the loss converges.

3.2 Learning with Transparent Initialization

Although some semantic segmentation datasets, such as PASCAL VOC and Berkeley benchmark, have no accurate edges for supervised learning, it can be compensated for by learnable contours from superpixel network on other datasets, such as SBDS500 (Arbelaez et al. 2010), for edge detection. Due to the domain gap of these datasets, however, pretrained superpixel models are more desirable than learning from scratch to jointly train semantic segmentation network for a fast loss convergence. Thus, in our proposal, linear layers or convolutional layers with 1×1 kernels are added to fuse the outputs of superpixel and semantic segmentation networks. Either or both can be pretrained.

Now, selecting an appropriate initialization on these additional layers is important to avoid interrupting the effect of learned parameters of the pretrained networks. A straightforward scheme is to cast the layer operations as an identity mapping between input and output at the early training stage. Net2Net (Chen, Goodfellow, and Shlens 2016) achieves it by using identity matrices to initialize linear layers. This method, however, is inefficient in learning since the identity matrices will result in highly sparse gradients. Also, it cannot handle negative hidden layers when activation functions are applied to the linear layers.

In contrast, we introduce transparent initialization with non-zero initialization values for dense gradients while identically mapping the layer input and output to preserve the effect of learned parameters of the pretrained networks.

Single Layer. For a linear layer without activation as $\mathbf{y} = \mathbf{x}\mathbf{A} + \mathbf{b}$ with layer weights \mathbf{A} , bias \mathbf{b} , and input \mathbf{x} , it can be generalized as a matrix multiplication with $\tilde{\mathbf{y}} = [\mathbf{y}, 1]$ by

$$\tilde{\mathbf{y}} = \tilde{\mathbf{x}}\mathbf{M} = [\mathbf{x}, 1] \begin{bmatrix} \mathbf{A} & \mathbf{0} \\ \mathbf{b} & 1 \end{bmatrix}. \quad (3)$$

To recover layer output \mathbf{y} from input \mathbf{x} , a right-inverse of \mathbf{M} is necessary to form an identity mapping such that $\mathbf{y} = \mathbf{x}$ via $\tilde{\mathbf{y}} = (\tilde{\mathbf{x}}\mathbf{M})\mathbf{M}^{-1}$. Clearly, we have

$$\mathbf{M}^{-1} = \begin{bmatrix} \mathbf{A}^{-1} & \mathbf{0} \\ -\mathbf{b}\mathbf{A}^{-1} & 1 \end{bmatrix}. \quad (4)$$

Thus, it needs at least two layers with the latter one initialized by Eq. (4).

Condition: For a matrix $\mathbf{M} \in \mathbb{R}^{m \times n}$, a right-inverse of \mathbf{M} exists iff the rank of \mathbf{M} is m and $m \leq n$. Consequently, given a matrix $\mathbf{M} \in \mathbb{R}^{m_0 \times m_{k-1}}$ that consists of a sequence of $k-1$ affine matrices $\mathbf{M}_i : \mathbb{R}^{m_{i-1}} \rightarrow \mathbb{R}^{m_i}$, where $i \in \mathcal{K} = \{1, \dots, k-1\}$, a right-inverse of $\mathbf{M}_1\mathbf{M}_2\dots\mathbf{M}_{k-1}$ exists iff $m_0 \leq m_i, \forall i \in \mathcal{K}$.

Multiple Layers. Existence of a right-inverse matrix relies on the condition above. This is also applied to k layers of Eq. (3) as $\tilde{\mathbf{y}} = \tilde{\mathbf{x}}\mathbf{M} = \tilde{\mathbf{x}}\mathbf{M}_1\mathbf{M}_2\dots\mathbf{M}_{k-1}\mathbf{M}_k$. For each

$M_i, \forall i \in \mathcal{K} = \{1, \dots, k-1\}$, the number of rows cannot be less than the columns after matrix multiplication between every two sequential layers. Initialization of $M_i, \forall i \in \mathcal{K}$ follows any standard approaches, normal distribution in our case. Then, the last layer is initialized by

$$M_k = (M_1 M_2 \dots M_{k-1})^{-1} \quad (5)$$

such that $\tilde{\mathbf{y}} = \tilde{\mathbf{x}}\mathbf{M} = \mathbf{x}$ due to $(M_1 M_2 \dots M_{k-1})M_k = \mathbf{I}$.

With Activation. Considering the nonlinearity of network by an activation function $\sigma(\cdot)$, such as ReLU, the affine transformation is now $\mathbf{y} = \sigma(\mathbf{x}\mathbf{A} + \mathbf{b})$.

Again, remember that for those k layers without activation, the goal of $\mathbf{x}_k = \mathbf{x}_0$ is to ensure Eq. (5). With an activation function, however, it can be rewritten as $\mathbf{x}_k = \sigma(\sigma(\tilde{\mathbf{x}}_0 M_1) M_2) \dots M_k$, which is simplified as

$$\mathbf{x}_k = \tilde{\mathbf{x}}_0 M_1 \sigma M_2 \sigma \dots M_k. \quad (6)$$

Nevertheless, note that matrix multiplication with respect to $\sigma(\cdot)$ is impossible as $\sigma(\cdot)$ is over unpredictable hidden layers and \mathbf{x} but not just M_i .

Now, we introduce our approach of the identity mapping between input and output of a linear layer with an activation function, for instance, ReLU in our case. Given the *first layer* with parameters $M_1 = [\mathbf{A}_1, \mathbf{b}_1]^T$, we denote the output without activation as $\mathbf{x}_1 = \mathbf{x}_0 \mathbf{A}_1 + \mathbf{b}_1$ and the output with activation as $\mathbf{x}'_1 = \sigma([\mathbf{x}_1, -\mathbf{x}_1])$, it follows that

$$\begin{aligned} \mathbf{x}_1 &= \sigma(\mathbf{x}_1) - \sigma(-\mathbf{x}_1) \\ &= \sigma([\mathbf{x}_1, -\mathbf{x}_1]) \begin{bmatrix} \mathbf{I} \\ -\mathbf{I} \end{bmatrix} \\ &= \sigma\left([\mathbf{x}_0, \mathbf{1}] \begin{bmatrix} \mathbf{A}_1 & -\mathbf{A}_1 \\ \mathbf{b}_1 & -\mathbf{b}_1 \end{bmatrix}\right) \begin{bmatrix} \mathbf{I} \\ -\mathbf{I} \end{bmatrix} \\ &= \sigma([\mathbf{x}_0, \mathbf{1}] \hat{M}_1) \begin{bmatrix} \mathbf{I} \\ -\mathbf{I} \end{bmatrix} = \mathbf{x}'_1 [\mathbf{I}, -\mathbf{I}]^T, \end{aligned} \quad (7)$$

where \mathbf{x}'_1 is the layer output and \hat{M}_1 is the initialized layer parameters for the first linear layer.

Next, with $M_2 = [\mathbf{A}_2, \mathbf{b}_2]^T$ for the second layer, we have

$$\begin{aligned} \mathbf{x}_2 &= \sigma([\mathbf{x}_2, -\mathbf{x}_2]) \begin{bmatrix} \mathbf{I} \\ -\mathbf{I} \end{bmatrix} \\ &= \sigma\left([\mathbf{x}_1, \mathbf{1}] \begin{bmatrix} \mathbf{A}_2 & -\mathbf{A}_2 \\ \mathbf{b}_2 & -\mathbf{b}_2 \end{bmatrix}\right) \begin{bmatrix} \mathbf{I} \\ -\mathbf{I} \end{bmatrix} \\ &= \sigma\left(\left[\mathbf{x}'_1 \begin{bmatrix} \mathbf{I} \\ -\mathbf{I} \end{bmatrix}, \mathbf{1}\right] \begin{bmatrix} \mathbf{A}_2 & -\mathbf{A}_2 \\ \mathbf{b}_2 & -\mathbf{b}_2 \end{bmatrix}\right) \begin{bmatrix} \mathbf{I} \\ -\mathbf{I} \end{bmatrix} \\ &= \sigma\left(\left[\mathbf{x}'_1 \begin{bmatrix} \mathbf{A}_2 & -\mathbf{A}_2 \\ -\mathbf{A}_2 & \mathbf{A}_2 \end{bmatrix} + \mathbf{b}_2, \mathbf{x}'_1 \begin{bmatrix} -\mathbf{A}_2 \\ \mathbf{A}_2 \end{bmatrix} - \mathbf{b}_2\right]\right) \begin{bmatrix} \mathbf{I} \\ -\mathbf{I} \end{bmatrix} \\ &= \sigma\left([\mathbf{x}'_1, \mathbf{1}] \begin{bmatrix} \mathbf{A}_2 & -\mathbf{A}_2 \\ -\mathbf{A}_2 & \mathbf{A}_2 \\ \mathbf{b}_2 & -\mathbf{b}_2 \end{bmatrix}\right) \begin{bmatrix} \mathbf{I} \\ -\mathbf{I} \end{bmatrix} \\ &= \sigma([\mathbf{x}'_1, \mathbf{1}] \hat{M}_2) \begin{bmatrix} \mathbf{I} \\ -\mathbf{I} \end{bmatrix} = \mathbf{x}'_2 [\mathbf{I}, -\mathbf{I}]^T, \end{aligned} \quad (8)$$

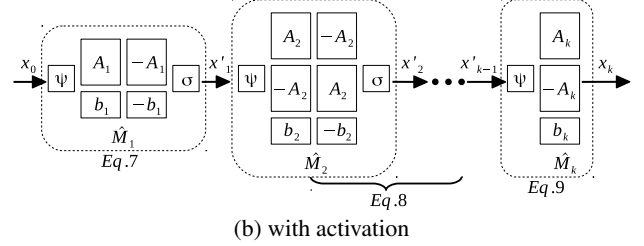
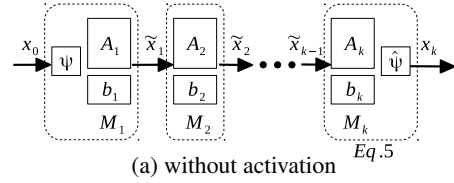


Figure 3: Transparent initialization. $\psi : \mathbf{x} \rightarrow [\mathbf{x}, \mathbf{1}]$; $\hat{\psi} : [\mathbf{x}, \mathbf{1}] \rightarrow \mathbf{x}$; σ : activation function. The order of (a) is in “Multiple Layers” and the order of (b) is in Eq. 10.

where \mathbf{x}'_2 is the layer output and \hat{M}_2 is the initialized parameters of this layer. This initialization is applied to the *middle layers*, that is for layers at $i \in \{2, \dots, k-1\}$.

For the *last layer* with parameter $M_k = [\mathbf{A}_k, \mathbf{b}_k]^T$, since its output is not followed by an activation function, it has

$$\begin{aligned} \mathbf{x}_k &= \mathbf{x}'_{k-1} \begin{bmatrix} \mathbf{I} \\ -\mathbf{I} \end{bmatrix} \mathbf{A}_k + \mathbf{b}_k = [\mathbf{x}'_{k-1}, \mathbf{1}] \begin{bmatrix} \mathbf{A}_k \\ -\mathbf{A}_k \\ \mathbf{b}_k \end{bmatrix} \\ &= \mathbf{x}'_k \hat{M}_k, \end{aligned} \quad (9)$$

where \hat{M}_k is the initialized parameters of the last layer.

Now, by extending layer parameters M_i to $\hat{M}_i, \forall i \in \{1, \dots, k\}$ by Eqs. (7)-(9) and ψ making $\mathbf{x}_i \rightarrow [\mathbf{x}_i, \mathbf{1}]$, operations turn from Eq. 6 to

$$\mathbf{x}_k = (((\mathbf{x}_0) \psi \hat{M}_1 \sigma) \psi \hat{M}_2 \sigma) \dots \psi \hat{M}_k = \mathbf{x}_0, \quad (10)$$

because each \mathbf{x}'_i (i.e., output with activation) can be recovered to \mathbf{x}_i (i.e., output without activation) and the initialization of the last layer satisfies Eq. (5).

Fig. 3 vividly demonstrates our transparent initialization for the additional layers without and with an activation function. In more details, we first adopt random initialization with normal distribution on $M_i, \forall i \in \{1, \dots, k-1\}$, followed by M_k initialized by Eq. 5 (Fig. 3a). Next, with an activation, the parameter dimensions are extended from M_i to $\hat{M}_i, \forall i \in \{1, \dots, k\}$, which are then initialized with values from $[\mathbf{A}_i, \mathbf{b}_i]^T$ in M_i (Fig. 3b).

Additionally, for other activation functions, such as LeakyReLU, the recovery of \mathbf{x} from $\sigma(\mathbf{x})$ requires

$$\mathbf{x} = \frac{1}{1 + \delta} [\sigma(\mathbf{x}), \sigma(-\mathbf{x})] \begin{bmatrix} \mathbf{I} \\ -\mathbf{I} \end{bmatrix}, \quad (11)$$

where $\delta > 0$ is the negative slope of LeakyReLU. Therefore, the substitution of Eq. (11) to Eqs. (7)-(8) contributes to the identity mapping in our transparent initialization. One can derive it in a similar way of ReLU in this section.

superpixel index	pixel index						
	0	1	2	3	4	...	N_p-1
0	0	1	1	0	0	...	0
1	0	0	0	1	1	...	0
2	1	0	0	0	0	...	1
...
N_s-1	0	0	0	0	0	...	0
sum	1	1	1	1	1	...	1

Table 1: Example of sparse property for indexing N_p pixels by N_s superpixels. Each superpixel contains only a few pixels (“1” in each row) for logit uniformization. Hence, an efficient encoding can be achieved by a sparse $N_s \times N_p$ matrix with N_p non-zero elements.

3.3 Logit Uniformization with Sparse Encoder

In addition to the notations of pixel number N_p , superpixel number N_s , and subsets of pixels $\mathcal{P} = \{\mathcal{P}_0, \dots, \mathcal{P}_{N_s-1}\}$ in Sec. 3.1, the label set is defined as $\mathcal{L} = \{0, \dots, N_l-1\}$ given N_l labels. For logit x_s^l of \mathcal{P}_s for superpixel s at label l , the logit uniformization follows

$$x_s^l(p) \leftarrow \frac{1}{|\mathcal{P}_s|} \sum_{p \in \mathcal{P}_s} x_s^l(p), \quad \forall p \in \mathcal{P}_s, \quad (12)$$

which guarantees all pixels in \mathcal{P}_s having the same logit at each label so as to be assigned with the same label.

Nevertheless, considering the high complexity of indexing $x_s^l(p)$, a dense matrix operation requires a large GPU memory, that is $N_l N_s N_p$, especially for the back-propagation in CNN learning. This makes it infeasible for training due to the limited GPU memory in our experiments.

Hence, we adopted a sparse encoder, including sparse encoding and decoding, with sparse matrix operations for the uniformization. Let us set matrix for indexing pixels by superpixel as $M(s, p)$, logit matrix as $M(l, p)$, where $s \in \mathcal{S}$, $p \in \mathcal{P}$, and $l \in \mathcal{L}$, sparse encoding and decoding are

$$\text{Encoding: } M(s, l) = \frac{\text{SMM}(M(s, p), M^T(l, p))}{\text{SADD}_{p \in \mathcal{P}_s}(M(s, p))}, \quad (13a)$$

$$\text{Decoding: } M(l, p) \leftarrow \text{SMM}(M^T(s, l), M(s, p)), \quad (13b)$$

where $M(s, p) \in \mathcal{B}^{N_s \times N_p}$ is 0-1 binary as is in Table 1, SMM^* is sparse matrix multiplication, and SADD^* is sparse addition. This converts Eq. (12) from dense operations to sparse operations with reduced complexity from $N_l N_s N_p$ to $N_l N_p$.

Without this sparse encoder to largely reduce the memory, it is infeasible to jointly train the networks due to the limited GPU memory in our experiments.

4 Experiments

We first evaluated the properties of our transparent initialization including its effectiveness of data recovery and numerical stability. Then, we demonstrated its effect on jointly learning pretrained networks of semantic segmentation and superpixel segmentation together with a sparse encoder for logit uniformization. Our code will be released upon publication with a user-friendly PyTorch module of the transparent initialization.

4.1 Properties of Transparent Initialization

Effectiveness. Our transparent initialization aims at identically mapping the output of linear layer(s) to the input at an early stage when finetuning pretrained network(s). It remains the effect of learned parameters of pretrained model(s) without losing the effectiveness of learned parameters. Off-the-shelf parameter initialization methods, such as random (uniform) and Xavier (Glorot and Bengio 2010) initialization, lead to random values of the output at the early training stage, which cannot generate effective features by the pretrained models. Also, compared with the identical initialization with identity matrices for deeper networks in Net2Net (Chen, Goodfellow, and Shlens 2016), our transparent initialization has a high initialization rate with much more non-zero parameters for dense gradients in backpropagation.

We evaluated these methods on 3 fully-connected layers. The (in_channels, out_channels) for each layer is (42, 64)→(64, 64)→(64, 42). Since Net2Net only supports square linear layer, *i.e.*, in_channels equals out_channels, to increase network depth, all layers have 42 in_channels and out_channels. Input data is normally distributed with size (4, 42, 512, 512), *i.e.*, (batch, in_channels, height, width).

manner	init. rate↑	recovery rate↑		non-square filter
		w/o activation	w activation	
random	98.2	0.0	0.0	✓
Xavier	98.2	0.0	0.0	✓
Net2Net	2.3	100.0	50.0	✗
ours	99.9	100.0	100.0	✓

Table 2: Effectiveness of parameter initialization on 3 fully-connected (FC) layers for data recovery. “initialization rate”: percentage of non-zero (absolute value $> \epsilon$) parameters; “recovery rate”: percentage of outputs with the same (difference $< \epsilon$) values as inputs; “activation”: ReLU; “non-square filter”: a FC layer with different numbers of in and out channels. Inputs are in $[-10, 10]$. $\epsilon=1e-4$.

In Table 2, random and Xavier initialization have 98% initialization rate but cannot recover the output from its input, leading to 0% recovery rate. Net2Net has only 2% initialization rate and 50% recovery rate with ReLU which only recovers non-negative values. In contrast, our transparent initialization has a high initialization rate and 100% recovery rate by Eqs. 7-9 with ReLU.

Numerical Stability. Since the effect of our transparent initialization is distributed across layers and Eq. 4 is achieved by a pseudo-inverse matrix for a rank-deficient matrix, the hidden layer has round-off errors and the result of matrix multiplication of layer parameters is not strictly identical. We tested the numerical stability of our transparent initialization on 3 numerical orders in Table 3. Clearly, the max error between input and output is in proportion to the magnitude order of input values. For a pretrained model, however, its output is usually stable in a numerical range, such as probability in $[0, 1]$. One can easily enforce a numerical regularization if the model output is out of range.

	[-1, 1]	[-10, 10]	[-100, 100]	[-1000, 1000]
max error	$\sim 6.8\text{e-}6$	$\sim 6.6\text{e-}5$	$\sim 6.5\text{e-}4$	$\sim 6.6\text{e-}3$

Table 3: Stability of transparent initialization with 4 numerical orders, *i.e.*, 1, 10, 100, 1000. Layer parameters are consistent with Table 2.

4.2 Evaluation on Semantic Segmentation

Dataset. For semantic segmentation, we used the combined version of PASCAL VOC2012 (Everingham et al. 2014) and Berkeley benchmark (Martin et al. 2001) for 21 classes segmentation with 20 object classes and 1 background. This dataset has 1449 images from PASCAL VOC 2012 val set for validation and 10582 images for training. Meanwhile, MS-COCO (Lin et al. 2014) was used to pre-train the semantic segmentation network, *i.e.*, DeepLabV3+ in our case. It has 92516 images for training and 3899 images for validation, while 20 classes from the primary 80 classes were selected in accordance with PASCAL VOC.

The adopted superpixel network with FCN from (Yang et al. 2020) was trained on Berkeley Segmentation Data Set and Benchmarks 500 (BSDS500) (Arbelaez et al. 2010) containing 500 images with handcrafted ground truth edges.

Learning Scheme. To train DeepLabV3+ from scratch on the combined dataset above, we set Learning Rate (LR) for ResNet as 0.007 and for ASPP and decoder as 0.07; to train on MS-COCO, LR was set to 0.01 for ResNet and 0.1 for others. LR for superpixel network pretrained on BSDS500 was the same as ResNet. ResNet was pretrained on ImageNet, which is accessible in PyTorch model zoo.

For jointly training pretrained DeepLabV3+ and superpixel with FCN, LR was $1\text{e-}6$ while the one for transparent initialization was $1\text{e-}7$ if adopted. No LR schedule was used for the 20-epoch joint training while “poly” decreasing LR schedule was used for 60 epochs for other training. The optimizer is SGD with momentum 0.9 and weight decay $5\text{e-}4$.

Experimental analysis. Since superpixel with FCN has multiple maxpooling, we used 512^2 crop size in training to easily recover the original size from decoders. Hence, evaluations by mIoU on both 512^2 and the original size were provided in Table 4.

We first reproduced DeepLabV3+ with ResNet101 backbone, resulting in 78.85% mIoU comparable to 78.43% in the code¹. Applying superpixel network over it by logit uniformization increased the mIoU by 0.37%. We then adopted a deeper ResNet, ResNet152, for a qualified baseline with 77.78% on the full size to evaluate our proposal.

Applying superpixel contours increased the mIoU from 77.78% to 78.15%, based on which finetuning using our transparent initialization further increased it by 0.79% (1.16% to the baseline). By pretrained on MS-COCO for PASCAL VOC 2012, our proposal still works with 0.61% increase of mIoU. This increase seems small because most edges in the ground truth were neglected (with white color in Fig. 4(d)) in the evaluation while our goal is to preserve sharp object edges aligned with its superpixel contours. Nevertheless, visualization of the successful cases in

manner	DeepLabV3+	SP	TI	MS-COCO	mIoU(512^2 /full)
baseline	ResNet101	-	-	-	78.85 / 76.47
ours	ResNet101	✓	-	-	79.22 / 76.98
baseline	ResNet152	-	-	-	79.32 / 77.78
ours	ResNet152	✓	-	-	79.94 / 78.15
	ResNet152	✓	✓	-	80.46 / 78.94
baseline	ResNet152	-	-	✓	82.62 / 80.76
ours	ResNet152	✓	✓	✓	83.39 / 81.37

Table 4: PASCAL VOC 2012 *val set*. “SP”: superpixel with logit uniformization; “TI”: transparent initialization. “mIoU” is on 512^2 image size used in training and full size.

Fig. 4 vividly show the enhanced object edges, especially when the objects and background have high contrastive intensities, such as bird wings and human heads.

5 Conclusion

In this paper, we proposed a joint learning scheme of semantic segmentation with superpixel contours to preserve object edges with transparent initialization and sparse encoder. The proposed transparent initialization is used to finetune the pretrained models with the effect of learned parameters by identically mapping the network output to its input at the early stage in learning. It is robust and more effective and efficient to recover data in linear layers than other parameter initialization methods, such as Net2Net. Meanwhile, the sparse encoder enables the feasibility of an efficient training with largely reduced GPU memories. Evaluation on PASCAL VOC 2012 dataset validates the effectiveness of our proposal in semantic segmentation with sharp object edges. Additionally, the proposed transparent initialization can also be applied to knowledge transfer on deeper pretrained networks with additional fully-connected layers.

References

- Achanta, R.; Shaji, A.; Smith, K.; Lucchi, A.; Fua, P.; and Susstrunk, S. 2012. SLIC Superpixels Compared to State-of-the-Art Superpixel Methods. *TPAMI* 34(11): 2274–2282.
- Achanta, R.; and Susstrunk, S. 2017. Superpixels and Polygons using Simple Non-iterative Clustering. *CVPR*.
- Arbelaez, P.; Maire, M.; Fowlkes, C.; and Malik, J. 2010. Contour Detection and Hierarchical Image Segmentation. *TPAMI* 33(5): 898–916.
- Badrinarayanan, V.; Kendall, A.; and Cipolla, R. 2017. SegNet: A Deep Convolutional Encoder-Decoder Architecture for Image Segmentation. *TPAMI* 39(12): 2481–2495.
- Bergh, M.; Boix, X.; Roig, G.; and Gool, L. 2015. SEEDS: Superpixels Extracted via Energydriven Sampling. *IJCV*.
- Chen, L.; Barron, J.; Papandreou, G.; Murphy, K.; and Yuille, A. 2016. Semantic Image Segmentation with Task-Specific Edge Detection using CNNs and a Discriminatively Trained Domain Transform. *CVPR*.
- Chen, L.; Papandreou, G.; Kokkinos, I.; Murphy, K.; and Yuille, A. 2017. DeepLab: Semantic Image Segmentation with Deep Convolutional Nets, Atrous Convolution, and Fully Connected CRFs. *TPAMI* 40(4): 834–848.

¹<https://github.com/jfzhang95/pytorch-deeplab-xception.git>

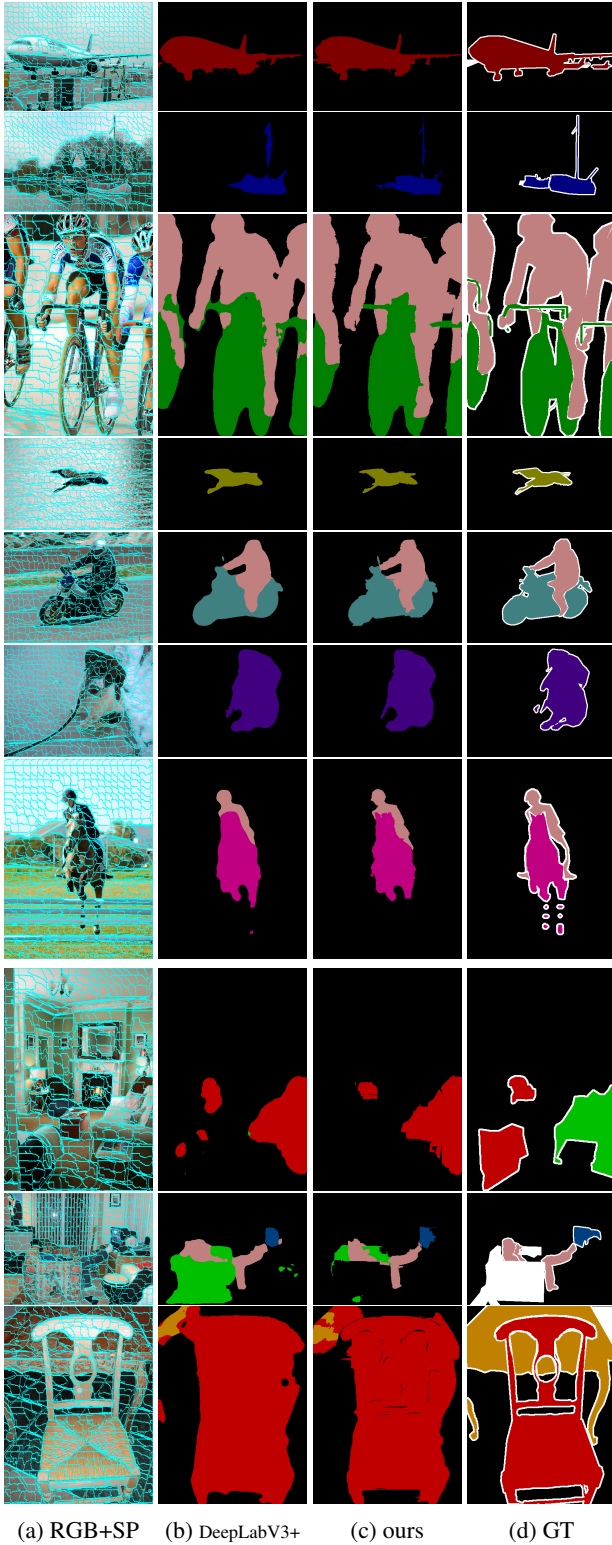


Figure 4: Examples on PASCAL VOC 2012 *val* set. The first 7 rows are successful cases; the last 3 rows are failure cases. SP contours are in blue in (a). Best view by zooming in.

Chen, L.; Zhu, Y.; Papandreou, G.; Schroff, F.; and Adam, H. 2018a. Encoder-Decoder with Atrous Separable Convolution for Semantic Image Segmentation. *ECCV*.

Chen, T.; Goodfellow, I.; and Shlens, J. 2016. Net2Net: Accelerating Learning via Knowledge Transfer. *ICLR*.

Chen, Y.; Kalantidis, Y.; Li, J.; Yan, S.; and Feng, J. 2018b. A2-nets: Double Attention Networks. *NeurIPS*.

Deng, J.; Dong, W.; Socher, R.; Li, L.; Li, K.; and Li, F. 2009. ImageNet: A Large-Scale Hierarchical Image Database. *CVPR*.

Everingham, M.; Eslami, S.; Gool, L.; Williams, C.; Winn, J.; and Zisserman, A. 2014. The PASCAL Visual Object Classes Challenge a Retrospective. *IJCV*.

Feng, D.; Schutz, C.; Rosenbaum, L.; Hertlein, H.; Glaser, C.; Tim, F.; Wiesbeck, W.; and Dietmayer, K. 2020. Deep Multi-Model Object Detection and Semantic Segmentation for Autonomous Driving: Datasets, Methods, and Challenges. *IEEE Transactions on Intelligent Transportation systems* 1–20.

Fu, J.; Liu, J.; Tian, H.; Li, Y.; Bao, Y.; Fang, Z.; and Lu, H. 2019. Dual Attention Network for Scene Segmentation. *CVPR*.

Gadde, R.; Jampani, V.; Kiefel, M.; Kappler, D.; and Gehler, P. 2016. Superpixel Convolutional Networks using Bilateral Inceptions. *ECCV*.

Glorot, X.; and Bengio, Y. 2010. Understanding the Difficulty of Training Deep Feedforward Neural Networks. *AISTATS*.

Gould, S.; Zhao, J.; He, X.; and Zhang, Y. 2014. Superpixel Graph Label Transfer with Learned Distance Metric. *ECCV*.

He, K.; Zhang, X.; Ren, S.; and Sun, J. 2016. Deep Residual Learning for Image Recognition. *CVPR*.

Hofmarcher, M.; Unterthiner, T.; Medina, J.; Klambauer, G.; Hochreiter, S.; and Nessler, B. 2019. Visual Scene Understanding for Autonomous Driving using Semantic Segmentation. *Explainable AI. LNCS* 11700: 285–296.

Hong, S.; Yan, X.; Huang, T.; and Lee, H. 2018. Learning Hierarchical Semantic Image Manipulation Through Structured Representations. *NeurIPS*.

Huang, G.; Liu, Z.; Maaten, L.; and Weinberger, K. 2017. Densely Connected Convolutional Networks. *CVPR*.

Isola, P.; Zoran, D.; Krishnan, D.; and Adelson, E. 2014. Crisp Boundary Detection using Pointwise Mutual Information. *ECCV*.

Jampani, V.; Sun, D.; Liu, M.; Yang, M.; and Kautz, J. 2018. Superpixel Sampling Networks. *ECCV*.

Jordan, M. 1998. Learning in Graphical Models. *MIT Press*.

Krahenbuhl, P.; and Koltun, V. 2011. Efficient Inference in Fully Connected CRFs with Gaussian Edge Potentials. *NeurIPS*.

- Li, X.; Zhong, Z.; Wu, J.; Yang, Y.; Lin, Z.; and Liu, H. 2019. Expectation-Maximization Attention Networks for Semantic Segmentation. *ICCV* .
- Li, Z.; and Chen, J. 2015. Superpixel Segmentation using Linear Spectral Clustering. *CVPR* .
- Lin, G.; Milan, A.; Shen, C.; and Reid, I. 2017. RefineNet: Multi-Path Refinement Networks for High Resolution Semantic Segmentation. *CVPR* .
- Lin, T.; Maire, M.; Belongie, S.; Bourdev, L.; Girshick, R.; Hays, J.; Perona, P.; Ramanan, D.; Zitnick, C.; and Dollar, P. 2014. Microsoft COCO: Common Objects in Context. *ECCV* .
- Liu, Y.; Yu, C.; Yu, M.; and He, Y. 2015. Manifold SLIC: A Fast Method to Compute Content-Sensitive Superpixels. *CVPR* .
- Long, J.; Shelhamer, E.; and Darrell, T. 2015. Fully Convolutional Networks for Semantic Segmentation. *CVPR* .
- Martin, D.; Fowlkes, C.; Tal, D.; and Malik, J. 2001. A Database of Human Segmented Natural Images and its Application to Evaluating Segmentation Algorithms and Measuring Ecological Statistics. *ICCV* .
- Mottaghi, R.; Chen, X.; Liu, X.; Cho, N.; Lee, S.; Fidler, S.; Urtasun, R.; and Yuille, A. 2014. The Role of Context for Object Detection and Semantic Segmentation in the Wild. *CVPR* .
- Park, H.; Jeong, J.; Yoo, Y.; and Kwak, N. 2017. Superpixel-Based Semantic Segmentation Rained by Statistical Process Control. *BMVC* .
- Salscheider, N. 2019. Simultaneous Object Detectin and Semantic Segmentation. *International conference on pattern recognition applications and methods (ICPRAM)* .
- Schroff, F.; Criminisi, A.; and Zisserman, A. 2008. Object Class Segmentation using Random Forests. *BMVC* .
- Schuermans, M.; Berman, M.; and Blaschko, M. 2018. Efficient Semantic Image Segmentation with Superpixel Pooling. *arXiv preprint arXiv:1806.02705* .
- Simonyan, K.; and Zisserman, A. 2015. Very Deep Convolutional Networks for Large-Scale Image Recognition. *ICLR* .
- Stutz, D.; Hermans, A.; and Leibe, B. 2018. Superpixels: An Evaluation of the State-of-the-Art. *CVIU* .
- Thoma, M. 2016. A Survey of Semantic Segmentation. *arXiv:1602.06541* .
- Tu, W.; Liu, M.; Jampani, V.; Sun, D.; Chien, S.; Yang, M.; and Kautz, J. 2018. Learning Superpixels with Segmentation-Aware Affinity Loss. *CVPR* .
- Uziel, R.; Ronen, M.; and Freifeld, O. 2019. Bayesian Adaptive Superpixel Segmentation. *ICCV* .
- Wang, P.; Zeng, G.; Gan, R.; Wang, J.; and Zha, H. 2013. Structure-Sensitive Superpixels via Geodesic Distance. *IJCV* .
- Wang, X.; Wang, T.; and Bu, J. 2011. Color Image Segmentation using Pixel Wise Support Vector Machine Classification. *pattern recognition* .
- Xing, F.; Cambria, E.; Huang, W.; and Xu, Y. 2016. Weakly Supervised Semantic Segmentation with Superpixel Embedding. *ICIP* .
- Yang, F.; Sun, Q.; Jin, H.; and Zhou, Z. 2020. Superpixel Segmentation with Fully Convolutional Networks. *CVPR* .
- Zhao, H.; Shi, J.; Qi, X.; Wang, X.; and Jia, J. 2017. Pyramid Scene Parsing Network. *CVPR* .
- Zhao, H.; Zhang, Y.; Liu, S.; Shi, J.; Loy, C.; Lin, D.; and Jia, J. 2018. PSANet: Point-wise Spatial Attention Network for Scene Parsing. *ECCV* .
- Zheng, S.; Jayasumana, S.; Paredes, B.; Vineet, V.; Su, Z.; Du, D.; Huang, C.; and Torr, P. 2015. Conditional Random Fields as Recurrent Neural Networks. *ICCV* .